

Laminar Flow Across a Bank of Low Aspect Ratio Micro Pin Fins

Ali Koşar

Chandan Mishra

Yoav Peles¹

Department of Mechanical, Aerospace and Nuclear Engineering, Rensselaer Polytechnic Institute, Troy, NY 12180

Pressure drops and friction factors associated with the forced flow of de-ionized water over staggered and in-line circular/diamond shaped micro pin-fin bundles 100 μm long with hydraulic diameter of 50 and 100 μm have been experimentally investigated over Reynolds number ranging from 5 to 128. Pin fins were arranged according to two different horizontal and vertical pitch ratios (1.5 and 5). The applicability of conventional scale correlations to evaluate micro flow tests results has been assessed. It is shown that the available large-scale correlations do not adequately predict the pressure drop obtained at the micro scale. A modified correlation, based on the experimental results obtained using micro scale devices, has been proposed. The refined correlation accounts for fin density and the endwall effects encountered in micro scale configurations. [DOI: 10.1115/1.1900139]

Introduction

Recent advances in microfabrication technology have resulted in a surge in Micro-Electro-Mechanical Systems (MEMS) research for various heat and mass transfer applications. In the last half decade, forced flow over a bank of pin fins (tubular or non-tubular) in MEMS devices has received increasing attention for applications such as micro chemical reactors [1], micro rockets [2,3], and micro biological systems [4]. Fluid flow over a bank of pins results in a characteristic pressure drop, which is often used as a criterion to optimally design heat transfers systems like heat exchangers [5]. A literature survey reveals numerous instances of experimental and numerical studies aspiring to estimate the pressure drop for fluid flow over pin fin–tube bundles using various geometrical fin configurations in conventional scale systems. It is therefore tempting to use scaled down versions of conventional models to predict hydrodynamic properties arising out of fluid flow across a bank of micro pin fins. However, various studies on fluid flow in MEMS devices have shown unexpected phenomena and deviations from established large scale results. Additional difficulties are encountered while attempting to adopt conventional scale correlations to model micro devices since micro fins in cross flow tend to be shorter (aspect ratio smaller than ~ 8) than the recommended height for ideal tube bundles in large scale systems [6], primarily because as size diminishes heat transfer coefficient surges, which results in lower fin efficiencies and thus shorter pin fins are desired. Moreover limited data is available for laminar flow of intermediate size tubes ($8 > H/D > 1/2$) at the conventional scale, and large deviations (up to 50%) have been observed between various empirical pressure drop correlations in conventional scale studies.

Over the past century, numerous studies have investigated various aspects of flow across conventional sized tube bundles. Pressure drop data for water and air in circular, rectangular, and oval tubes collected primarily through experimental studies have been employed to develop friction factor correlations for laminar, transitional, and turbulent flows. The developed correlations have been widely used to ameliorate the design of large scale systems. Gaddis and Gnielski [6] proposed general correlations for laminar, turbulent, and transition regions for long tubes ($H/D > 8$) using data obtained from previous experimental studies of pressure drop. The correlations included the effects of fluid temperature,

number of rows of tubes, and tube geometrical configurations. Sparrow and Grannis [7] studied air flow across staggered forward-facing vertex diamond-shaped pin fins (45 deg and 90 deg) over Reynolds numbers based on the fin hydraulic diameter ranging from 20 to 2200 and noticed high friction factors in the 45 deg arrangement for low Reynolds number ($\text{Re} < 100$). At higher Reynolds numbers, the inertial effects dominate and the friction factor increased for the 90 deg arrays. The authors employed the experimental data to propose friction factor correlations for a variety of geometrical configurations. Chyu et al. [8] studied heat transfer and pressure drop characteristics for circular, cubic, and diamond fin arrays in a narrow channel for both in-line and staggered arrangements, and they concluded that cube arrays are the best arrangement for heat exchangers because of their enhanced heat transfer characteristics and moderate pressure losses. Ruth [9] compared the performance of lenticular with circular cross section tube banks in cross flow and reported a 20% increase in the ratio between the Stanton number and the friction coefficient for the lenticular pins for $2 \times 10^4 < \text{Re} < 5 \times 10^4$. The increase has been attributed to the lower accelerations and pressure gradients of the lenticular configuration, which results in reduced separation and drag. Sara [10] studied the effect of tip clearance ratio and inter-fin distance on pressure drop in flow across square cross-section pin fins in a staggered arrangement for Reynolds numbers ranging from 1×10^4 to 3.4×10^4 and observed that a decrease in the clearance ratio results in a decrease in the friction factor. Correlations involving the prediction of the friction factor have been presented in this article.

Flows over intermediate size pin fin banks are commonly used in turbine cooling systems to increase the internal heat transfer characteristics. The pin height-to-diameter ratios of typical heat sink used for such applications are between 1/2 and 4 [11]. Damerow et al. [12] measured pressure drops in channels with arrays of pin fins having H/D from 2 to 4 with various pin spacing geometries and found no H/D effect on the friction factor. A similar trend has been reported by Metzger et al. [13], who also obtained friction factors data, which agreed well with the long tube correlations proposed by Jacob [14]. Armstrong and Winstanley [15] compared the experimental data obtained by Peng [16], Metzger et al. [13], Damerow et al. [12], and Jacob [14]. The correlation proposed by Metzger et al. [13] provided the best fit for the data (within $\pm 15\%$), while Damerow's [12] correlation did not match the experimental results. Although Jacob's [14] correlation was originally developed for long fins, it predicted the experimental data fairly well. An interesting result that might explain the similar pressure drop trends for long and intermediate size tubes was obtained by Sparrow et al. [17], who studied the

¹Corresponding author. Telephone: 518-276-2886; Fax: 518-276-2623; E-mail: pelesy@rpi.edu

Contributed by the Fluids Engineering Division for publication in the JOURNAL OF FLUIDS ENGINEERING. Manuscript received: July 29, 2004. Final manuscript received: February 19, 2005. Associate Editor: M. Volkan Otugen.

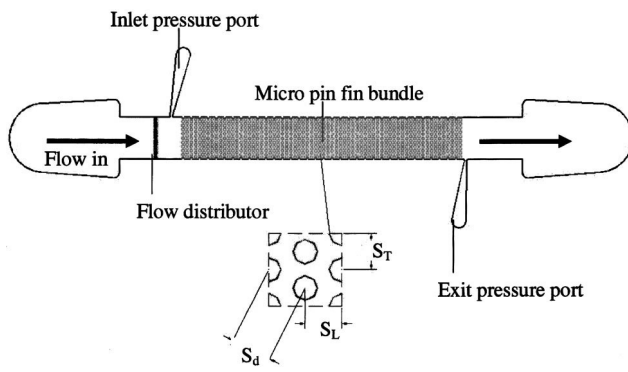


Fig. 1 CAD model of pin fin array

endwall effect of cross flow over a cylinder attached to a wall for Reynolds numbers ranging from 3500 to 23,000. Wall–cylinder interaction was found to be confined to within one diameter from the wall, and the interaction height was Reynolds number dependent. Low Reynolds number flows result in thicker interaction heights than high Reynolds number flow. Since the correlations cited above were developed based on transitional and turbulent flow data, no apparent dependency on H/D was found. However, Short et al. [5,18] showed that the friction factors over intermediate size tubes are strongly dependent on the height-to-diameter ratio for laminar flows but not for turbulent flows.

The aforementioned studies provide valuable insight into the pressure drop characteristics of fluid flow across a bank of pin fins at the conventional scale. It is not clear if the correlations and prediction tools developed for conventional scale systems are applicable to micro devices. Moreover, scaling studies have not been conducted to validate these correlations in the micro scale. In addition, the data on friction factor for intermediate size cylinders (and noncylindrical pin fins) at the conventional scale is limited and primarily available for transitional and turbulent flows ($Re > 1000$). Therefore, there is a strong need for conducting experimental studies on the pressure drop in cross flows over various micro pin fin bundles to either validate the correlations available from conventional scale studies or dispute their utility at the micro scale. The present study investigates pressure drops due to flow of water over staggered and in-line micro pin fin bundles. Micro scale results are compared with the existing large scale data and the conventional scale correlations are assessed in terms of their ability to predict pressure drop characteristics in micro flows. Finally, a modified correlation, which includes endwall effects, is proposed for flows over micro pin fin bundles.

Device Fabrication and Experimental Procedure

MEMS Device Design. The microchannels employed in the present study are fabricated using techniques adapted from semiconductor manufacturing. The process flow is very flexible and allows the creation of different fin geometries (circular, square, diamond, etc.) inside the microchannel. Positioning of the pin arrays in both staggered and in-line arrangements is achieved by simply incorporating these features into the masks. The fins are arranged inside a $1500\text{ }\mu\text{m}$ wide microchannel of depth $100\text{ }\mu\text{m}$ as shown in the CAD model in Fig. 1.

A double side polished, n -type $\langle 100 \rangle$ single crystal silicon wafer is processed on both sides to create a microfluidic device, which consists of a microchannel embedded with an array of fins. Pressure tapings are created at appropriate places on the device (Fig. 1). At first, the top side and bottom side masks are designed and fabricated. A $1\text{ }\mu\text{m}$ thick thermal oxide is deposited on both sides of the silicon wafer to protect the bare wafer surface. The top side mask pattern is transferred onto the silicon wafer through a photolithography step. The resist pattern on the wafer protects areas,

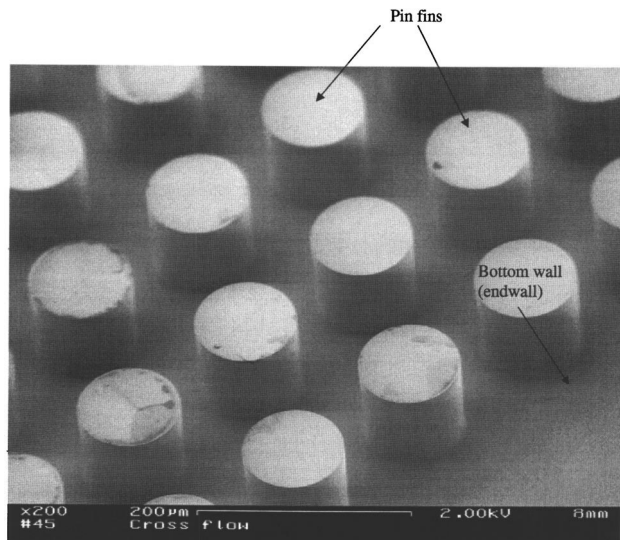


Fig. 2 SEM image of pin fins bundle

which are not to be etched during the DRIE (deep reactive ion etching) process. A subsequent RIE (reactive ion etching) process is used to remove oxide in places not protected by the resist. The wafer is then etched in a DRIE process and silicon is removed up to a depth of $100\text{ }\mu\text{m}$ forming the microchannel containing pin fin bundles along with the pressure ports and the inlet and exit ports of the device. The DRIE process forms deep vertical trenches on the silicon wafer with a characteristic scalloped sidewall possessing a peak-to-peak roughness of $\sim 0.3\text{ }\mu\text{m}$. Once top side processing is completed, the resist is stripped and the wafer is flipped for bottom side processing. The wafer is again taken through a photolithography, RIE step but the bottom mask is employed instead and the mask pattern is transferred on to the other side of the wafer. Finally, a DRIE process is used to etch the silicon and create openings for the inlet, the exit, and the pressure ports. Subsequent wet bench processing removes all oxide and resist on the wafer. The completed silicon wafer is anodically bonded to a 1 mm thick Pyrex wafer to seal the microchannels. The processed stack is finally diced to separate the devices from the parent wafers and prepare them for packaging and interfacing with the experimental setup. An SEM image of the actual device is shown in Fig. 2 and a CAD model is presented in Fig. 1 displaying the fin bundles and the pressure ports on the device.

Experimental Setup Design. The experimental setup is classified into three major subsystems: (a) The test section, (b) the flow subsystem, and (c) the instrumentation and data acquisition subsystem. A detailed layout of the experimental setup is provided in Fig. 3.

The test section consists of microchannels and an opposite packaging module to facilitate the transit of fluids through the micro device and to allow pressure measurements at different locations via the ports in the device. The packaging module consists of three components: (a) A transparent top plate, (b) a bottom plate with alignment pins, and (c) an adapter plate.

The bottom plate houses a number of o-rings for fluidic sealing while the alignment pins are provided to facilitate the easy positioning of microchannels. The adapter plate compensates for any die-saw errors and the transparent polycarbonate top plate allows flow visualization during test runs. The silicon device is compressed against the gaskets (o-rings) by the top and the bottom plate to forge the fluidic seals. This setup ensures hermetic sealing and offers access to the fluidic connections (inlet, outlet, and pressure ports) of the micro device through the bottom block.

The flow subsystem includes an inlet and an exit pressure

Experimental Setup

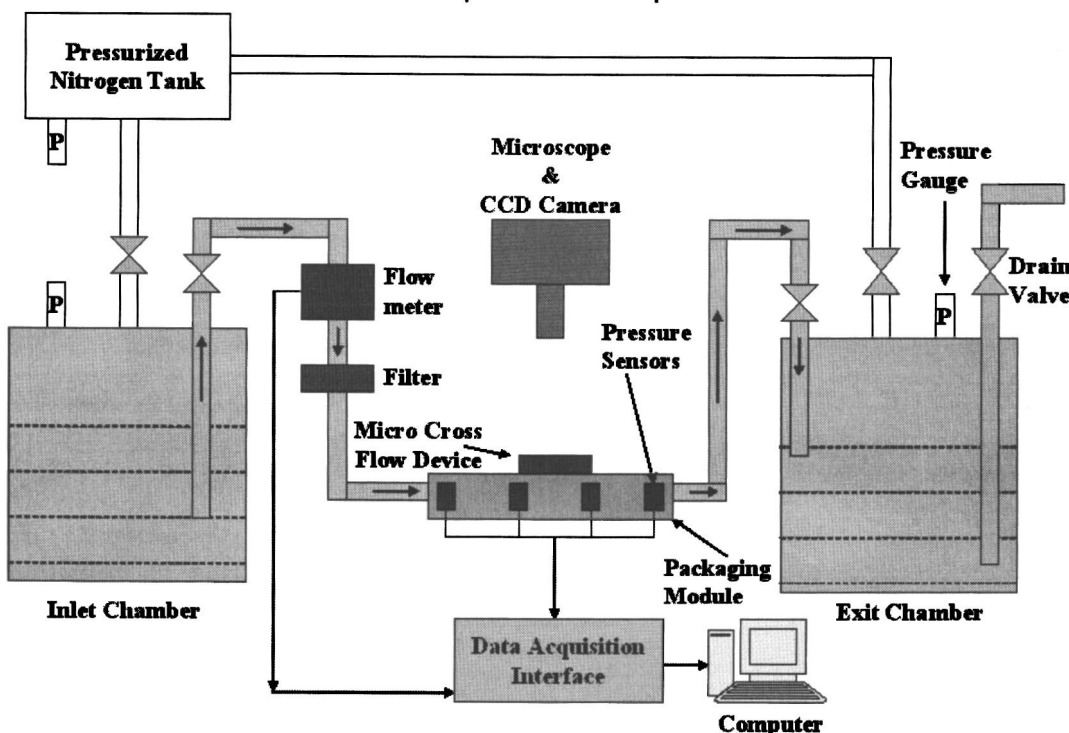


Fig. 3 Experimental setup

chamber capable of withstanding pressures up to 190 Psi and all plumbing to and from the test section. The fluidic connections to the test section from the pressurized tanks are established through appropriate stainless steel fittings. A pressure difference between the inlet and the exit chambers causes a flow through the microchannel. The inlet chamber is pressurized with filtered dry nitrogen and filtered de-ionized water is the working fluid in all experiments. The de-ionized water is delivered through a calibrated flow meter and a $0.2 \mu\text{m}$ filter is introduced before the test rig to depurate the fluid and avoid any clogging of the microfluidic device. Air is removed from the flow circuit by a Welch vacuum pump before any de-ionized water is introduced into the microchannel.

The instrumentation and data acquisition subsystem consists of a few precision pressure transducers, which are mounted on the bottom plate of the packaging through appropriate fittings. Pressure data is obtained at various locations in the microchannel through the pressure ports created inside the microfluidic device (Fig. 1). The pressure sensors deliver data to a PC based LABVIEW® data acquisition subsystem, which collects and stores the data for further analysis. The working liquid is not recirculated in any of the experiments and is collected in the exit chamber.

Experimental Procedure. The flow rate is induced by the pressure difference between the inlet and exit chambers and it can also be controlled by a fine adjustment ball valve located upstream of the test section (Fig. 3). Experiments are conducted over a wide range of inlet pressures and pressure gauges are used to monitor the pressure inside the inlet chambers. All experiments are performed at room temperature (22°C) and no heat is supplied to the devices, maintaining adiabatic conditions. The exit chamber is kept at atmospheric pressure throughout the experiments and the de-ionized water temperature is continuously monitored. The inlet chamber pressure is increased in a controlled manner and pressure and flow rate data are collected from various pressure and flow sensors through the LABVIEW® interface and stored for further

analysis. The pressure drop caused by the flow over a bank of pin fins is detected by the pressure transducers for the desired flowrate and data is collected only after reaching steady state conditions.

Data Reduction and Uncertainty Analysis

Data Reduction. Friction factor f is obtained from the following expression:

$$f_{\exp} = \frac{(P_{\text{in}} - P_{\text{exit}})2\rho_F}{N_{\text{row}} G^2} \quad (1)$$

where the mass flux (G) is calculated based on the minimum cross-sectional flow area using the expression

$$G = \frac{\dot{Q} \rho_F}{A_{\min}} \quad (2)$$

The Reynolds number and the minimum cross-sectional flow area are usually calculated using two different approaches depending on the pin height-to-diameter ratio. For arrays with long fins ($H/D > 8$), referred in this paper as “tube bundle” fins, the pressure drop (and heat transfer) is dominated by the fin while the endwall effects are secondary [19]. In this approach, the length scale for calculating the Reynolds number is simply the fin hydraulic diameter. Very short fins ($H/D < 1/2$) are commonly used in compact heat exchangers, where the characteristic pressure drop is severely influenced by the top and bottom walls. These fin configurations are referred as “compact heat exchanger” fins in this paper. This approach utilizes the hydraulic diameter of the heat exchanger for calculating the Reynolds number.

The Reynolds number and A_{\min} for the “tube bundle” approach for in-line and staggered fin configuration are expressed as follows:

Table 1 Uncertainties in variables used in uncertainty analysis (friction factor)

Uncertainty	Error (%)
Flow rate, Q (for each reading)	1
Experimental inlet and exit pressure	0.25
Tube hydraulic diameter, D	1
Channel width, w	1
Channel height, H	0.67
Density of the fluid, ρ_F	0.5
G	3.8
f	7.2

for in-line configuration

$$Re = \frac{G D}{\mu} \quad (3)$$

for staggered configuration

$$A_{\min} = \frac{S_T - D}{S_T} w H \quad (4)$$

$$A_{\min} = \frac{2(S_d - D)}{S_T} w H \text{ for } \frac{S_T + D}{2} < S_d \quad (5)$$

$$A_{\min} = \frac{2(S_d - D)}{S_T} w H \text{ for } \frac{S_T + D}{2} > S_d \quad (6)$$

The Reynolds number for the “compact heat exchanger” approach is given by:

$$Re_d = \frac{G d_h}{\mu} \quad (7)$$

where

$$d_h = \frac{4 A_{\min} L}{A} \quad (8)$$

and

$$A = \pi D H N_t + 2 \left(w L - \frac{\pi D^2}{4} N_t \right) \quad (9)$$

For in-line tube configuration:

$$A_{\min} = N H (S_T - D) \quad (10)$$

For staggered tube configuration:

Table 2 Devices dimensions

Device	S_T/D	S_L/D	H/D	D (μm)	clearance (μm)
1SDS (Staggered, Diamond, 45°, of Small fin hydraulic diameter)	5	5	2	50	0
2SCL (Staggered, Circular, of Large fin hydraulic diameter)	1.5	1.5	1	100	0
3SCS (Staggered, Circular, of Small fin hydraulic diameter)	1.5	1.5	2	50	0
4ICL (In-line, Circular, of Large fin hydraulic diameter)	1.5	1.5	1	100	0

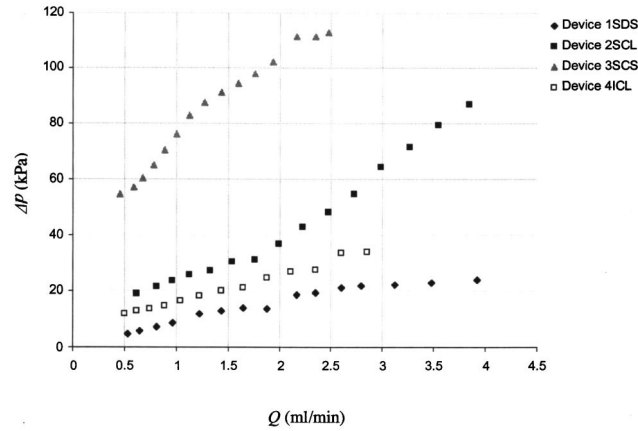


Fig. 4 Pressure drop vs flow rate for device 1SDS through 4SCL

$$A_{\min} = \left(\left(\frac{w}{S_T} - 1 \right) c + (S_T - D) \right) H \quad (11)$$

where

$$c = \begin{cases} S_T - D & \text{if } S_T - D < S_d - D \\ S_d - D & \text{if } S_d - D < S_T - D \end{cases}$$

The friction factor for the entire fin pin configuration is obtained from Eq. (1). The comparison of the experimental data with existing correlations is done through the mean absolute error (MAE), which is defined as:

$$MAE = \frac{1}{M} \sum_{i=1}^M \frac{|f_{\exp} - f_{\text{pred}}|}{f_{\text{pred}}} \times 100\% \quad (12)$$

Uncertainty Analysis. The uncertainties of the measured values are given in Table 1 and are derived from the manufacturer’s specification sheet while the uncertainties of the derived parameters are obtained using the propagation of uncertainty method developed by Kline and McClintock [20].

Results and Discussion

Pressure Drop. Four devices, listed in Table 2, are tested in this study, for which the pressure drops between the inlet and exit are shown in Fig. 4. The geometrical configurations of the selected four devices provide a measure (although limited in extent) of pin arrangement (staggered and in-line), aspect ratio, and pin shape. As expected, the pressure drop is higher for the denser

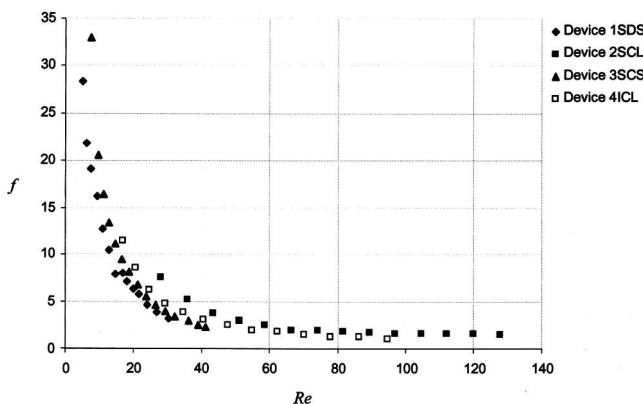


Fig. 5 Friction factors for "tube bundle" approach

configurations. Because of its smaller diameter, the Reynolds number based on the fin hydraulic diameter corresponding to the same flow rate is smaller for device 3SCS (Staggered, Circular, of Small fin hydraulic diameter) than for device 2SCL (Staggered, Circular, of Large fin hydraulic diameter). Consequently, the friction factor is higher and the pressure drop required to maintain the same flow rate is higher for device 3SCS. Due to the cylinder-wake interaction with increasing flow rate device 2SCL has increasing slope after a certain Q , while devices 3SCS and 1SDS have decreasing slopes. As expected the flow resistance of device 4ICL (In-line, Circular, of Large fin hydraulic diameter) is smaller than the staggered arrangements with the same fin diameter (device 2SCL). At high pitch-to-diameter ratio, the flow resistance drops (device 1SDS).

Trends in Experimental Friction Factor. Friction factors vs. Reynolds number profiles are given in Figs. 5 and 6 for "tube bundle" and "compact heat exchanger" approaches. The general trends of the experimental results are consistent with the effects of tube arrangement, and pitch ratio on friction factor for "tube bundle" approach in conventional scale.

Although the tube density of device 2SCL and 3SCS are the same, the friction factor is much larger for device 2SCL. For example using the "tube bundle" approach at $Re=28.0$ the friction factor for device 2SCL is $f=7.495$, while at $Re=29.30$ the friction factor for device 3SCS is $f=3.915$. Using the "compact heat exchanger" approach at $Re=25.25$ the friction factor for device 2SCL is $f=2.891$, while at $Re=25.35$ the friction factor for device 3SCS is $f=2.507$. The discrepancies between the friction factors are attributed to the differences in the height-to-diameter of the

two devices ($H/D=1$ for device 2SCL, and $H/D=2$ for device 3SCS). This, to some extent, contradicts most previous studies [12,13,16] which have found that H/D had no effect on the friction factor. However, Short et al. [5] have reported that the friction factor is dependent on H/D for laminar flows and this compares favorably with the current data. As discussed by Sparrow et al. [17] wall-fin interactions are confined to within one diameter of the wall for Reynolds number larger than 3500, and tend to diminish at higher Reynolds numbers. At lower Reynolds number, the wall boundary layer thickness extends a few tube diameters from the wall and can strongly affect the hydrodynamic field (and, therefore, the pressure drop) throughout the entire fin height. Note that to some respect the aspect ratio effect should have been accounted for by the use of the Reynolds number based on the "compact heat exchanger" approach. Indeed, for a given Reynolds number, the ratios between the friction factors of the two devices reduced. However, there are still considerable discrepancies between the values of the friction factors of the two devices.

Flow through staggered configuration is more tortuous than flow over an in-line arrangement, and as a result, larger friction factors are expected for staggered configuration. However, at low Reynolds numbers the ratio between the friction factor of similar tube diameters and pitch-to-diameter ratio are larger than for larger Reynolds numbers. As seen in Figs. 5 and 6, at Reynolds numbers below 40 the friction factors for device 2SCL are about 1.6 times larger than for device 4ICL, while at higher Reynolds number the ratio between the friction factors approaches unity. A similar trend was obtained by Short et al. [5] thereby emphasizing the fact that as Re increases, the effects of the arrangement (in-line versus staggered) on friction factor diminishes.

The friction factors of devices 1SDS and 3SCS are approximately equal for a range of Reynolds numbers although the density of device 1SDS having diamond shaped fins is about five times less than device 3SCS with circular fins for the "tube bundle" approach, whereas they are greater for the "compact heat exchanger" approach. This signifies the importance of the pin's shape. It can be inferred that diamond shaped fins result in considerably larger friction factors compared to circular fins, which is consistent with the finding of Chyu et al. [8]. This is because the sharp pointed regions of diamond shaped fins produce increased form drag on the pins, which results in larger friction factors.

Comparison Between Experimental and Conventional Friction Factor. A large number of correlations developed for long and short tubes are used to evaluate the friction factors. In the present study, ten long tube correlations and four intermediate size tube correlations are included, which are summarized in Table 3. Among the ten long tube correlations, four are specified as applicable only for laminar flow (1,4,6,11), four only for turbulent flow (2,3,5,7), and the remaining are either for all ranges, transition range, or some combination of two or more flow regimes. The experimental friction factors together with the calculated ones obtained from these correlations are presented in Tables 4 and 5. The mean absolute errors are presented in Tables 6 and 7. The correlation that results with the overall lowest MAE value is Sparrow and Grannis [7] correlation with an average MAE of 31.9% using the "tube bundle" approach. Although Sparrow and Grannis [7] correlation was obtained for air and recommended for diamond shaped tubes, it represents the data well particularly for the staggered arrangements. This might be since it was originally developed for Reynolds numbers similar to the current study and was based on tests from dense fin arrangements. It is also not surprising that the correlation provided the best prediction for the data of device 1SDS, which has relatively long ($H/D=2$) diamond shaped fin pins. Excluding the diamond shape configuration (device 1SDS) Gunter and Shaw [21] and the HEDH [22] correlations predicted the experimental data quite well. Gunther and Shaw [21] correlation predicted the friction factor for device 2SCL, 3SCS, and 4ICL with MAEs of 22.5%, 22.0%, and 17.1%, respectively, while for device 1SDS it underpredicted the data by

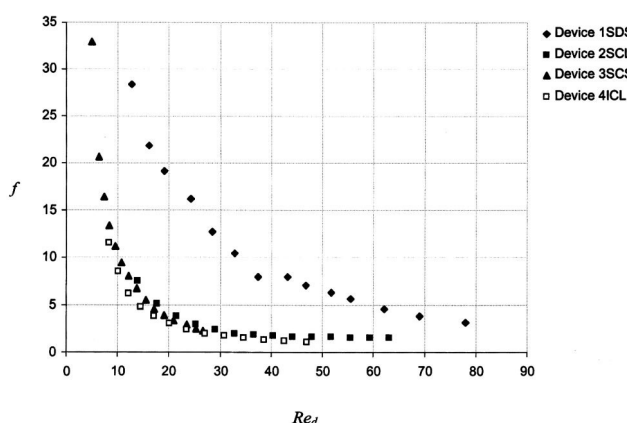


Fig. 6 Friction factors for "compact heat exchanger" approach

Table 3 Correlations for the friction factor and their mean absolute errors; Conventional scale friction factor correlations

Correlation	Reference	Fluid	Reynolds number	H/D	Configuration	Friction factor
1	Chilton and Generaux [24]	Air	Laminar region	Long tubes	Circular staggered	$f = \frac{106}{Re}$
2	Chilton and Generaux [24]	Air	Turbulent region	Long tubes	Circular Staggered inline	$f = \frac{C_c}{Re^{0.2}}$ $C_c = 3$ for in line tube configuration $C_c = 1.32$ for staggered tube configuration
3	Jacob [14]	Air	Turbulent region	Long tubes	Circular Staggered inline	For in-line configuration: $f = \frac{1}{Re^{0.15}} \left[0.176 + \frac{0.32(S_L/D)}{\left(\frac{S_T}{D} - 1\right)^{0.43+(1.13D/S_L)}} \right]$ For staggered configuration: $f = \frac{1}{Re^{0.16}} \left[1 + \frac{0.47}{\left(\frac{S_T}{D} - 1\right)^{1.08}} \right]$
4	Gunther and Shaw [21]	Air	Laminar region	Long tubes	Circular In-line Staggered	$f = \frac{180}{Re} \left(\frac{4 S_T S_L}{\pi D^2} - 1 \right)^{0.4} \left(\frac{D b_G}{S_T} \right)^{0.6}$ $b_G = \frac{S_L}{D}$ for in line tube configuration $b_G = \frac{S_d}{D}$ for staggered tube configuration
5	Gunther and Shaw [21]	Air	Turbulent region	Long tubes	Circular In-line Staggered	$f = \frac{1.92}{Re^{0.145}} \left(\frac{4 S_T S_L}{\pi D^2} - 1 \right)^{0.4} \left(\frac{D b_G}{S_T} \right)^{0.6}$ b_G is defined in the previous row
6	Bergelin et al. [25]	Mobile oil	Laminar region	Long tubes	Circular In-line Staggered	$f = \frac{280}{Re} \left(\frac{1}{a_B} \right)^{1.6}$ $a_B = \frac{S_T}{D}$ for in line tube configuration and for staggered configuration with $\frac{S_L}{D} \geq \sqrt{2 \frac{S_T}{D} + 1}$ $a_B = \frac{S_d}{D}$ for staggered tube configuration for staggered configuration with $\frac{S_L}{D} \leq \sqrt{2 \frac{S_T}{D} + 1}$
7	Damerow [12]	Air	Turbulent regime	Short tubes $2 < H/D < 4$	Airfoils	$f = [8.24(S_T/D)^{-1.1}] Re_D^{-0.16}$
8	Kast [26]	Air	Laminar and turbulent regime	Long tubes	Circular In-line Staggered	$f = \frac{128}{Re} + \frac{4}{Re^{0.16}}$

81.6%. Using the HEDH [22] correlation the MAE's for device 1SDS, 3SCS, and 4ICL are 17.4%, 25.8%, and 21.9%, respectively, whereas for device 1SDS the MAE is 99.5%. The higher friction factors values for the diamond shape pins are in accordance with conventional scale findings (Chyu et al. [8]).

Comparison between the results for device 1SDS and device 2SCL with Sparrow and Grannis correlation [7] reveals another important aspect of endwall effects [endwall effects account for the interaction between the pin fins and the base, on which they

reside (top and bottom walls)]. If endwall effects are neglected, the correlation should have resulted in higher friction factors for device 2SCL than the experimental data, since the pin fins in device 2SCL are circular and the correlation was developed for diamond shape pin fins. On the other hand, the correlation should have underpredicted the experiments results for device 1SDS since the pins are diamond shaped and the only discrepancy between the data used for correlation 12 and the current data (other than the scale) is endwall effects. However, the opposite occurs.

Table 3 (Continued.)

correlation	Reference	Fluid	Reynolds number	H/D	Configuration	Friction factor																		
9	Metzger et al. [13]	Air	1000-100000	Short tubes $H/D=1$	Rectangular Staggered Short tubes $H/D=1$, $P_T=2.5$, $P_L=1-5$	For $1000 < Re < 10000$ $f = 1.268 Re^{-0.132}$ For $10000 < Re < 100000$ $f = 7.04 Re^{-0.318}$																		
10	HEDH [22]	All fluids	All Re	Long tubes	Circular Both in-line and staggered	$f = 4b_1 \left(\frac{1.33}{S_T/D} \right)^b (Re)^b$ $b = \frac{b_3}{1 + 0.14(Re)^{b_4}}$																		
11	Gaddis and Gnielski [6]	All fluids	Laminar regime	Long tubes	Circular Both in-line and staggered	$f = \frac{280\pi \left[\left(\left(\frac{S_L}{D} \right)^{0.5} - 0.6 \right)^2 + 0.75 \right]}{\text{Re} \left(4 \frac{S_L S_T}{D^2} - \pi \right)^{1.6}}$ <p>where</p> $c = \frac{S_T}{D}$ for in line arrangement and a staggered arrangement with $\frac{S_L}{D} \geq \frac{1}{2} \sqrt{2 \frac{S_T}{D} + 1}$ $c = \frac{S_D}{D}$ for in line arrangement and a staggered arrangement with $\frac{S_L}{D} < \frac{1}{2} \sqrt{2 \frac{S_T}{D} + 1}$																		
12	Sparrow and Grannis [7]	Air	20-2200	Long tubes	Diamond 45° deg vertex 90° deg vertex $P_T=1.15-2$ $P_L=1-2$ staggered	For $P_L=0.866 P_T$ $f = \frac{127}{Re} + 0.90 \quad P_T < 1.35$ $f = \frac{88}{Re} + 0.70 \quad P_T \geq 1.35$ For $P_L=P_T$ $f = \frac{155}{Re} + 0.82 \quad P_T < 1.35$ $f = \frac{98}{Re} + 0.72 \quad P_T \geq 1.35$																		
13	Moores and Joshi [23]	Water	200-10000	Short Tubes $0.5 < H/D < 1$	Circular Staggered 1 $P_T=1.3-1.36$ $P_L=1.13-1.18$	$f = 4a_0 \left(\frac{H}{D} \right)^{a_1} \left(\frac{cl+H}{H} \right)^{a_2} Re^{a_3}$ <table border="1"><tr><td>$10^2 < Re < 10^3$</td><td>$10^3 < Re < 10^4$</td></tr><tr><td>a_0</td><td>4.76</td></tr><tr><td>a_1</td><td>-0.742</td></tr><tr><td>a_2</td><td>0.505</td></tr><tr><td>a_3</td><td>-0.502</td></tr><tr><td></td><td>3.2</td></tr><tr><td></td><td>-0.138</td></tr><tr><td></td><td>-0.183</td></tr><tr><td></td><td>-0.42</td></tr></table>	$10^2 < Re < 10^3$	$10^3 < Re < 10^4$	a_0	4.76	a_1	-0.742	a_2	0.505	a_3	-0.502		3.2		-0.138		-0.183		-0.42
$10^2 < Re < 10^3$	$10^3 < Re < 10^4$																							
a_0	4.76																							
a_1	-0.742																							
a_2	0.505																							
a_3	-0.502																							
	3.2																							
	-0.138																							
	-0.183																							
	-0.42																							
14	Short et al. [5]	Air	175-4500	Short Tubes $1.9 < H/D < 7.5$	Circular Staggered $S_T=1.3-1.36$ $S_L=2.0-6.4$	$f = 140.4 \left(\frac{S_L}{D} \right)^{-1.3} \left(\frac{S_T}{D} \right)^{-0.78} \left(\frac{H}{D} \right)^{-0.55} Re^{-0.65}$ for $Re < 1000$ $f = 0.884 \left(\frac{S_L}{D} \right)^{-1.4} \left(\frac{S_T}{D} \right)^{-0.54} \left(\frac{H}{D} \right)^{0.056} Re^{-0.08}$ for $Re \geq 1000$																		

The correlation underpredicted the experiment results for device 2SCL, and overpredicted results for device 1SDS. This suggests that endwall effects are significant for $H/D=1$, but much less important for $H/D=2$, and a shift from pressure drop dominated by endwall effects to pressure drop dominated by pin fin effects occurs at some value between $1 < H/D < 2$. The endwall effects are also apparent when comparing device 2SCL and 2SCS with Gunther and Shaw [21] correlation. At Reynolds number above ~ 25 the correlation overpredicted the experimental results for the relatively long pin fins of device 3SCS, while for device 2SCL the correlation underpredicted the results even at $Re=127.7$.

Moores and Joshi [23] poorly predicted the experimental data correlation. This is not surprising since their laminar region data also correlated poorly with their own correlation. Moreover, larger transverse and longitudinal pitches were used in their study, which

are beyond the recommended range for this correlation. From all the various studies considered here only Short et al. [5] addressed endwall effects on intermediate size pins. Therefore, it was expected that correlation 14 would agree well with the experimental results. However, the correlation did not predict the experimental data well even for the circular pins staggered array (for device 2SCL and 3SCS, the MAE's are 71.3% and 34.7%, respectively), and the prediction of the in-line array is much above the experimental data (for device 4ICL the MAE's is 99.1%).

The existing correlations best fit the data obtained from device 3SCS ($H/D=2$). This might further support the hypothesis that endwall effects are significant in the low Reynolds number range of the current experiments, especially when comparing the results obtained for device 2SCL ($H/D=1$). Since all correlations (except

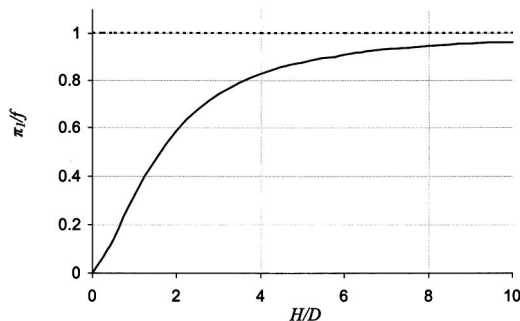


Fig. 7 π_1 to the total friction factor f [Eq. (13)] ratio versus H/D ratio at $Re=40$

correlations 13 and 14), assume long fins (including the one that was developed for the short fins) it is expected that their prediction capabilities will deteriorate for smaller H/D , where endwall effects become significant. However, for device 1SDS all correlations, except Sparrow and Grannis [7] generated much lower friction factors than experiments. This is somewhat surprising since device 1SDS has H/D similar to device 2SCL. Moreover it has been tested at higher Reynolds numbers (in comparison to the other devices) and endwall effects should have diminished. However, as discussed in previous sections conventional scale studies strongly suggest that friction factor across diamond shape pins are larger than circular pins.

Using the “compact heat exchanger” approach did not seem to improve the prediction results. Although three correlations (Gad-el-Hak and Gnielski [6], Chilton and Generaux [24], Bergelin et al. [25]) provided better predictions under the “compact heat exchanger” approach, the predictions of the other correlations in Tables 6 and 7 were poorer. Bergelin et al. [25] provided the best prediction with an average MAE of 41.7%. Chilton and Generaux [24] produced the largest improvement with the “compact heat exchanger” approach compared to the “tube bundle” approach (from an MAE of 68.4% to an MAE of 44.8%). Since it was recommended only for the laminar regime, the effects of the change in the approach were more pronounced and these effects played an improving role in the prediction of experiment data, for devices 2SCL, 3SCS, and 4ICL (MAEs are 28.0%, 35.6%, and 15.3%, respectively). It is difficult to draw a conclusion regarding the approach, which provides best overall approximation, since the average MAEs for all correlations are relatively large for both approaches.

In conclusion, the comparison of the test results with existing correlations provided relatively large discrepancies, and only the correlation presented by Short et al. [5] attempted to capture all the important physical parameters that derive the pressure drop across intermediate size fin pin banks at low Reynolds numbers. In the following section, the development of a more general correlation that will especially account for endwall effects is detailed.

Development of a New Correlation for Friction Factor. Based on the experimental results a friction factor correlation for flow across fin pin array was developed which accounts for endwall effect and fin density. The correlation has the following form:

$$f = \pi_1 + \pi_2 \quad (13)$$

where

$$\pi_1 = \frac{C_3}{Re^{k_1}} \left(\frac{H/D}{H/D + 1} \right)^{k_2} \left(\frac{S_T S_L}{A_C} \right)^{k_3} \text{ and;}$$

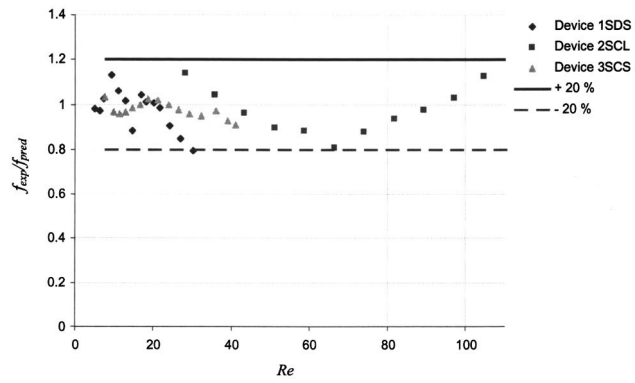


Fig. 8 Comparison between measured and calculated friction factors [Eq. (13)] for staggered configurations

$$\pi_2 = \frac{C_4}{Re^{k_5}} \left(\frac{1}{1 + H/D} \right)^{k_4} \left(\frac{S_T S_L}{A_C} \right)^{k_6}$$

C_3 , C_4 , k_1 , k_2 , k_3 , k_4 , and k_5 are constants, which minimize the prediction error of the experimental data. Using the least-square method similar to the procedure presented by Mathews [27], the values of these constants, which best fit the experimental data, are found and are listed in Table 8.

The first (π_1) and second (π_2) terms on the right hand side of Eq. (13) have a similar form to Gunther and Shaw [21] correlation and account for the friction on the fin and on the top and bottom walls, respectively. This hybrid approach to the representation of the friction factor acknowledges that neither Re nor Re_d alone can fully capture the physical parameters that govern friction factors at intermediate tube sizes. At large tube aspect ratio π_2 vanishes (the term powered by k_4 diminishes), and the pressure drops are mainly due to friction exerted on the pins. As the pins become shorter, π_1 diminishes (the term powered by k_2 diminishes), and the friction losses on the top and bottom walls, which are accounted by π_2 , gradually dominate. This trend is demonstrated in Fig. 7 for device 3SCS at $Re=40$. For $H/D=1$, π_1 is much smaller than π_2 . As H/D becomes larger, the ratio between π_1 and the total friction factor approaches unity. For $H/D > 5$, π_1 accounts for ~90% of the friction factor.

The correlation with the constant values of Table 8 predicted all friction factor data of the staggered arrangements with a MAE of 7.3%, while for in-line arrangement, the MAE is 2.7%. Table 9 lists all MAE's of Eq. (13). A comparison between the experimental data and the calculated friction factors obtained from Eq. (13) is given in Figs. 8 and 9, and as can be seen, almost all the data

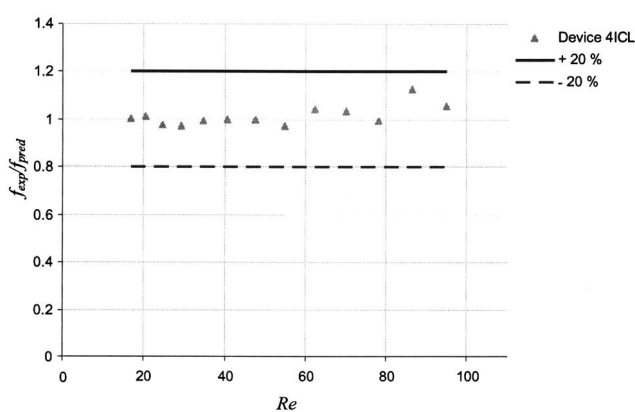


Fig. 9 Comparison between measured and calculated friction factors [Eq. (13)] for in-line configuration

Table 4 Friction factors using the “tube bundle” approach; Friction factors using the “tube bundle” approach

Device	<i>Re</i>	<i>Q</i> (ml/min)	<i>f_{Gaddis}</i>	<i>f_{Sparrow}</i>	<i>f_{Moores}</i>	<i>f_{Kast}</i>	<i>f_{Gunther}</i>	<i>f_{Chilton}</i>	<i>f_{Bergelin}</i>	<i>f_{Short}</i>	<i>f_{HEDH}</i>	<i>f_{Experiment}</i>
1SDS	30.29	3.924	0.07828	5.093	2.0544	2.793	0.7599	0.1136	0.02284	0.3674	0.035404	3.152
1SDS	26.83	3.476	0.08835	5.633	2.1832	2.953	0.8577	0.1282	0.02578	0.3975	0.034892	3.849
1SDS	24.12	3.125	0.09828	6.165	2.3032	3.107	0.954	0.1426	0.02868	0.426	0.03448	4.61
1SDS	21.55	2.792	0.11	6.793	2.4372	3.286	1.068	0.1596	0.0321	0.4583	0.034084	5.691
1SDS	20.07	2.6	0.1181	7.228	2.526	3.408	1.147	0.1714	0.03447	0.4801	0.03386	6.298
1SDS	18.15	2.351	0.1306	7.898	2.6568	3.594	1.268	0.1895	0.03812	0.5125	0.03358	7.069
1SDS	16.75	2.171	0.1415	8.48	2.7656	3.753	1.374	0.2053	0.04129	0.5398	0.033388	7.953
1SDS	14.5	1.878	0.1635	9.661	2.974	4.072	1.588	0.2373	0.04772	0.5931	0.033116	7.898
1SDS	12.75	1.652	0.1859	10.86	3.1716	4.39	1.805	0.2697	0.05425	0.6446	0.032968	10.44
1SDS	11.06	1.433	0.2143	12.38	3.4064	4.788	2.081	0.3109	0.06254	0.7071	0.032908	12.74
1SDS	9.433	1.222	0.2513	14.36	3.69	5.299	2.44	0.3646	0.07334	0.7842	0.03298	16.18
1SDS	7.418	0.961	0.3196	18.02	4.164	6.226	3.102	0.4636	0.09326	0.9167	0.0334	19.15
1SDS	6.26	0.811	0.3787	21.19	4.532	7.017	3.676	0.5494	0.1105	1.024	0.03394	21.84
1SDS	4.987	0.646	0.4754	26.37	5.08	8.295	4.615	0.6897	0.1387	1.187	0.03502	28.35
2SCL	127.7	3.846	0.701	1.894	1.6684	2.971	0.9698	0.4452	0.6148	2.582	1.0848	1.471
2SCL	120.1	3.615	0.7458	1.958	1.7208	3.06	1.032	0.4737	0.654	2.688	1.1468	1.522
2SCL	112.4	3.384	0.7966	2.03	1.7788	3.16	1.102	0.506	0.6986	2.806	1.2168	1.559
2SCL	104.8	3.154	0.8549	2.112	1.8432	3.274	1.183	0.543	0.7497	2.938	1.2968	1.617
2SCL	97.08	2.923	0.9224	2.208	1.9148	3.403	1.276	0.5859	0.8089	3.086	1.3884	1.602
2SCL	89.42	2.692	1.001	2.32	1.9956	3.554	1.386	0.6361	0.8783	3.256	1.4944	1.671
2SCL	81.75	2.461	1.095	2.453	2.0872	3.73	1.515	0.6957	0.9606	3.451	1.6196	1.771
2SCL	74.09	2.231	1.209	2.614	2.1932	3.94	1.672	0.7677	1.06	3.679	1.7688	1.859
2SCL	66.42	2	1.348	2.812	2.3168	4.195	1.865	0.8563	1.182	3.95	1.9508	1.935
2SCL	58.76	1.769	1.524	3.061	2.4636	4.513	2.109	0.968	1.337	4.278	2.1772	2.428
2SCL	51.09	1.538	1.753	3.386	2.6428	4.92	2.425	1.113	1.537	4.685	2.4672	2.891
2SCL	43.42	1.307	2.062	3.825	2.8676	5.464	2.853	1.31	1.808	5.207	2.8532	3.768
2SCL	35.76	1.077	2.504	4.452	3.1612	6.229	3.465	1.591	2.196	5.907	3.3952	5.124
2SCL	28.09	0.846	3.188	5.421	3.5684	7.394	4.41	2.025	2.795	6.91	4.216	7.495
3SCS	41.09	2.474	2.18	3.991	1.7628	5.668	3.015	1.384	1.911	3.687	2.9984	2.291
3SCS	39.04	2.351	2.294	4.153	1.8084	5.866	3.173	1.457	2.011	3.811	3.1384	2.507
3SCS	36.05	2.171	2.484	4.423	1.8824	6.195	3.437	1.578	2.179	4.014	3.3708	2.941
3SCS	32.14	1.935	2.786	4.851	1.994	6.711	3.854	1.769	2.443	4.324	3.7356	3.39
3SCS	29.3	1.764	3.057	5.235	2.0892	7.172	4.229	1.941	2.681	4.593	4.06	3.915
3SCS	26.51	1.596	3.378	5.69	2.1964	7.714	4.673	2.145	2.962	4.901	4.44	4.607
3SCS	23.8	1.433	3.763	6.236	2.3188	8.362	5.206	2.39	3.3	5.257	4.892	5.511
3SCS	21.16	1.274	4.233	6.902	2.46	9.147	5.856	2.688	3.712	5.675	5.436	6.703
3SCS	18.73	1.128	4.78	7.679	2.6148	10.06	6.614	3.036	4.192	6.142	6.068	8.08
3SCS	16.63	1.002	5.384	8.535	2.7756	11.06	7.449	3.42	4.721	6.636	6.752	9.412
3SCS	14.68	0.884	6.1	9.551	2.9552	12.23	8.439	3.874	5.349	7.197	7.56	11.19
3SCS	12.9	0.7765	6.944	10.75	3.154	13.62	9.607	4.41	6.09	7.829	8.5	13.39
3SCS	11.24	0.677	7.965	12.2	3.3788	15.28	11.02	5.059	6.985	8.56	9.628	16.41
3SCS	9.74	0.5865	9.194	13.94	3.6312	17.28	12.72	5.839	8.063	9.396	8.229	20.62
3SCS	7.54	0.454	11.88	17.74	4.128	21.61	16.43	7.543	10.42	11.1	13.86	32.93
4ICL	94.9	2.857	0.9437	2.238	1.9368	3.444	1.306	0.5994	0.8276	3.132	1.4168	1.041
4ICL	86.36	2.6	1.037	2.371	2.0308	3.62	1.435	0.6586	0.9094	3.33	1.542	1.25
4ICL	78.09	2.351	1.147	2.526	2.136	3.825	1.587	0.7284	1.006	3.556	1.6876	1.251
4ICL	70.12	2.111	1.277	2.711	2.2544	4.066	1.767	0.8112	1.12	3.813	1.8584	1.498
4ICL	62.38	1.878	1.436	2.936	2.3908	4.354	1.986	0.9118	1.259	4.115	2.0636	1.756
4ICL	54.87	1.652	1.632	3.214	2.55	4.706	2.258	1.037	1.431	4.472	2.3144	1.949
4ICL	47.6	1.433	1.881	3.568	2.7384	5.147	2.603	1.195	1.65	4.905	2.6284	2.43
4ICL	40.59	1.222	2.206	4.029	2.9664	5.714	3.052	1.401	1.935	5.44	3.0312	3.044
4ICL	34.61	1.042	2.587	4.569	3.2136	6.372	3.58	1.643	2.269	6.034	3.496	3.815
4ICL	29.36	0.884	3.05	5.225	3.49	7.16	4.22	1.937	2.675	6.715	4.052	4.741
4ICL	24.65	0.742	3.633	6.053	3.8108	8.145	5.027	2.308	3.186	7.524	4.74	6.176
4ICL	20.43	0.615	4.384	7.117	4.188	9.399	6.065	2.784	3.844	8.501	5.612	8.519
4ICL	16.74	0.504	5.349	8.486	4.628	11	7.401	3.398	4.691	9.675	6.716	11.53

fall within $\pm 20\%$ of the correlation. All the data for the in-line device was within $\pm 10\%$ of the correlation, whereas about 75% of the data for the devices in staggered configuration fall within $\pm 10\%$.

Conclusions

In this study, friction factor measurements are obtained for micro scale flows across a variety of 100 μm long pin fins of 50 and 100 μm hydraulic diameter in both in-line and staggered configurations having two different transverse and horizontal pitch ratios (1.5 and 5) over Reynolds number ranging from 5 to 128. Both the “tube bundle” and “compact heat exchanger” approaches have been employed to evaluate the friction factors and the pressure drops. Experimental results showed that correlations available for

conventional scale systems could not fully predict the pressure drops obtained at the micro scale. A new correlation has been proposed to account for the fin density and the endwall effects at the micro scale. The main conclusions drawn from this investigation are presented below:

- (1) Existing conventional scale correlations are not able to predict the pressure drops accurately. A mean absolute error of more than 30% has been observed for all correlations examined in this study.
- (2) From the large number of conventional scale correlations only very few provide the correct ground for comparison. This is because pin fins are relatively short in micro scale systems and the flow is predominantly laminar. Surpris-

Table 5 Friction factors using the “compact heat exchanger” approach

Device	<i>Re</i>	<i>Q</i> (ml/min)	<i>f_{Gaddis}</i>	<i>f_{Sparrow}</i>	<i>f_{Moores}</i>	<i>f_{Kast}</i>	<i>f_{Gunther}</i>	<i>f_{Chilton}</i>	<i>f_{Bergelin}</i>	<i>f_{Short}</i>	<i>f_{HEDH}</i>	<i>f_{Experiment}</i>
1SDS	78.01	3.924	0.03039	2.528	1.2776	1.829	0.295	0.04409	0.008869	0.1986	0.039004	3.152
1SDS	69.11	3.476	0.0343	2.738	1.358	1.898	0.333	0.04977	0.01001	0.2149	0.038308	3.849
1SDS	62.13	3.125	0.03816	2.944	1.4324	1.963	0.3704	0.05536	0.01114	0.2303	0.037684	4.61
1SDS	55.51	2.792	0.04271	3.188	1.5156	2.038	0.4146	0.06196	0.01246	0.2478	0.03702	5.691
1SDS	51.69	2.6	0.04586	3.357	1.5708	2.088	0.4452	0.06654	0.01338	0.2595	0.036604	6.298
1SDS	46.74	2.351	0.05072	3.617	1.6524	2.163	0.4924	0.07359	0.0148	0.2771	0.036024	7.069
1SDS	43.15	2.171	0.05494	3.843	1.72	2.227	0.5333	0.07971	0.01603	0.2919	0.035576	7.953
1SDS	37.34	1.878	0.06349	4.301	1.8496	2.352	0.6164	0.09212	0.01853	0.3207	0.034788	7.898
1SDS	32.84	1.652	0.07218	4.767	1.9728	2.475	0.7007	0.1047	0.02106	0.3485	0.034132	10.44
1SDS	28.49	1.433	0.08321	5.358	2.1184	2.627	0.8078	0.1207	0.02428	0.3823	0.03346	12.74
1SDS	24.3	1.222	0.09758	6.127	2.2948	2.817	0.9472	0.1416	0.02848	0.424	0.032788	16.18
1SDS	19.11	0.961	0.1241	7.547	2.5892	3.156	1.204	0.18	0.03621	0.4956	0.031964	19.15
1SDS	16.12	0.811	0.147	8.776	2.8192	3.44	1.427	0.2133	0.04291	0.5535	0.031532	21.84
1SDS	12.84	0.646	0.1846	10.79	3.1604	3.89	1.792	0.2678	0.05386	0.6416	0.031176	28.35
2SCL	63.14	3.846	1.418	2.911	2.3764	4.322	1.962	0.9009	1.244	4.082	2.0412	1.471
2SCL	59.35	3.615	1.509	3.04	2.4516	4.486	2.088	0.9584	1.323	4.25	2.1576	1.522
2SCL	55.56	3.384	1.612	3.186	2.534	4.67	2.23	1.024	1.413	4.436	2.2888	1.559
2SCL	51.77	3.154	1.73	3.353	2.6252	4.88	2.393	1.099	1.517	4.645	2.438	1.617
2SCL	47.98	2.923	1.866	3.547	2.7276	5.121	2.582	1.185	1.637	4.88	2.6096	1.602
2SCL	44.19	2.692	2.026	3.774	2.8424	5.401	2.803	1.287	1.777	5.148	2.8088	1.671
2SCL	40.41	2.461	2.216	4.043	2.9732	5.732	3.066	1.408	1.944	5.456	3.0436	1.771
2SCL	36.62	2.231	2.446	4.368	3.124	6.128	3.384	1.553	2.145	5.817	3.324	1.859
2SCL	32.83	2	2.728	4.769	3.3	6.612	3.774	1.733	2.392	6.245	3.6656	1.935
2SCL	29.04	1.769	3.084	5.273	3.5096	7.218	4.266	1.959	2.704	6.763	4.092	2.428
2SCL	25.25	1.538	3.546	5.93	3.7648	7.999	4.907	2.253	3.11	7.407	4.64	2.891
2SCL	21.46	1.307	4.173	6.817	4.084	9.047	5.773	2.65	3.659	8.232	5.368	3.768
2SCL	17.67	1.077	5.067	8.086	4.504	10.53	7.01	3.218	4.444	9.34	6.396	5.124
2SCL	13.88	0.8458	6.45	10.05	5.084	12.81	8.923	4.096	5.656	10.93	7.952	7.495
3SCS	26.67	2.474	3.357	5.661	2.19	7.681	4.645	2.132	2.944	4.882	4.416	2.291
3SCS	25.35	2.351	3.533	5.911	2.2468	7.976	4.888	2.244	3.098	5.046	4.624	2.507
3SCS	23.4	2.171	3.827	6.327	2.3384	8.469	5.295	2.431	3.356	5.315	4.968	2.941
3SCS	20.87	1.935	4.292	6.986	2.4772	9.245	5.937	2.726	3.764	5.726	5.504	3.39
3SCS	19.02	1.764	4.709	7.578	2.5952	9.939	6.515	2.991	4.129	6.082	5.984	3.915
3SCS	17.21	1.596	5.203	8.279	2.7284	10.76	7.198	3.305	4.563	6.49	6.548	4.607
3SCS	15.45	1.433	5.796	9.12	2.8804	11.73	8.02	3.682	5.083	6.962	7.22	5.511
3SCS	13.74	1.274	6.52	10.15	3.0556	12.92	9.02	4.141	5.718	7.515	8.028	6.703
3SCS	12.16	1.128	7.364	11.34	3.2484	14.3	10.19	4.677	6.458	8.134	8.968	8.08
3SCS	10.8	1.002	8.294	12.66	3.448	15.82	11.47	5.268	7.273	8.788	9.988	9.412
3SCS	9.53	0.884	9.396	14.23	3.6712	17.61	13	5.968	8.24	9.53	11.192	11.19
3SCS	8.372	0.7765	10.7	16.07	3.918	19.71	14.8	6.794	9.381	10.37	12.596	13.39
3SCS	7.299	0.677	12.27	18.3	4.196	22.25	16.98	7.793	10.76	11.34	14.28	16.41
3SCS	6.323	0.5865	14.16	20.98	4.512	25.29	19.59	8.995	12.42	12.44	16.288	20.62
3SCS	4.895	0.454	18.29	26.85	5.128	31.91	25.31	11.62	16.04	14.7	20.624	32.93
4ICL	46.9	2.857	1.909	3.608	2.7588	5.196	2.642	1.213	1.674	4.952	2.6632	1.041
4ICL	42.68	2.6	2.098	3.875	2.8924	5.526	2.903	1.333	1.84	5.265	2.8976	1.25
4ICL	38.59	2.351	2.32	4.191	3.0424	5.912	3.21	1.474	2.035	5.622	3.1712	1.251
4ICL	34.65	2.111	2.584	4.565	3.2116	6.366	3.575	1.641	2.266	6.029	3.492	1.498
4ICL	30.83	1.878	2.905	5.019	3.4056	6.914	4.019	1.845	2.547	6.505	3.878	1.756
4ICL	27.12	1.652	3.302	5.583	3.632	7.587	4.569	2.097	2.896	7.071	4.352	1.949
4ICL	23.52	1.433	3.807	6.299	3.9008	8.436	5.267	2.418	3.338	7.756	4.944	2.43
4ICL	20.06	1.222	4.464	7.231	4.224	9.532	6.176	2.835	3.915	8.601	5.704	3.044
4ICL	17.11	1.042	5.235	8.324	4.576	10.81	7.243	3.325	4.591	9.54	6.584	3.815
4ICL	14.51	0.884	6.171	9.652	4.972	12.35	8.538	3.919	5.412	10.62	7.64	4.741
4ICL	12.18	0.742	7.352	11.33	5.428	14.28	10.17	4.669	6.447	11.9	8.952	6.176
4ICL	10.1	0.615	8.87	13.48	5.964	16.75	12.27	5.634	7.779	13.44	10.62	8.519
4ICL	8.274	0.504	10.82	16.25	6.592	19.91	14.97	6.874	9.492	15.3	12.732	11.53

Table 6 MAE's (%) of the correlations for each device using the “tube bundle” approach

Device	Gaddis and Gnielski [6]	Sparrow and Grannis [17]	Moores and Joshi [23]	Kast [26]	Gunther and Shaw [21]	Chilton and Generaux [24]	Bergelin et al. [25]	Short et al. [5]	HEDH [22]
1SDS	98.1	17.9	63.9	50.0	81.6	97.3	99.4	93.0	99.5
2SCL	44.0	28.9	19.6	85.5	22.5	64.4	50.7	71.3	17.4
3SCS	34.1	30.6	59.0	56.0	22.0	58.2	42.2	34.7	25.8
4ICL	26.6	51.8	41.8	111.6	17.1	53.4	35.6	99.1	21.9
Overall	50.8	31.9	46.4	74.5	35.9	68.4	57.1	73.4	41.2

Table 7 MAE's (%) of the correlations for each device using the “compact heat exchanger” approach

Device	Gaddis and Gnielski [6]	Sparrow and Grannis [17]	Moores and Joshi [23]	Kast [26]	Gunther and Shaw [21]	Chilton and Generaux [24]	Bergelin et al. [25]	Short et al. [5]	HEDH [22]
1SDS	99.3	48.4	29.4	70.4	92.9	98.9	99.8	96.2	98.0
2SCL	16.1	104.4	51.6	187.0	56.8	28.0	11.5	169.0	53.7
3SCS	22.9	63.2	49.1	107.9	44.1	35.6	22.0	44.6	36.6
4ICL	49.5	151.5	72.6	240.5	105.6	15.3	34.4	210.8	94.1
Overall	46.5	90.3	50.3	149.1	73.8	44.8	41.7	127.2	69.6

- ingly very few correlations are available for such pin fin configurations and flow regime. The correlations, which are applicable, provided large deviations from experimental results. At this point it is not clear whether this discrepancy is due to the limited data obtained in conventional scale, which is applicable to micro scale configuration and flow conditions or whether the differences arise from inherent scale effects.
- (3) Pin fin height to diameter ratio has a significant effect on the friction factor. The device with lower H/D ratio produces higher friction factors at the same tubes densities and Reynolds number. The H/D ratio effect reduces with increasing Reynolds number. A similar trend was observed by Short et al. [5].
 - (4) A new correlation accounting for the fin density and end-wall effects has been developed for in-line circular, staggered circular, and staggered diamond shaped pin fin arrangements. The proposed correlation predicted the experimental data with MAEs of 2.7%, 7.4%, and 7.2% for in-line circular, staggered circular, and staggered diamond shaped pin fins arrangements, respectively. For large H/D ratios ($H/D > 8$), the correlation converges to a long tube type correlation while small H/D ratios transform it to short tube correlations.
 - (5) Staggered tube configuration results in higher friction factors than the in-line configuration. This trend has also been observed in conventional scale studies. The difference between the friction factors obtained from different arrangements diminishes with the increase in the Reynolds number.
 - (6) The diamond shaped tubes produce higher friction factors when compared with the circular tubes. This is consistent with the results obtained by Chyu et al. [8] in their conventional scale experiments.

Table 8 Constant values for Eq. (13) that best fits experimental results

	staggered arrangement (circular fin pins)	staggered arrangement (diamond shaped fin pins)	in-line arrangement
C_3	1739	1126	7259
C_4	345	6.6	54
k_1	1.7	1.1	1.7
k_2	1.1	1.5	1.9
k_3	-0.3	-0.4	-0.4
k_4	2.0	1.7	2.0
k_5	1.0	0.7	0.7
k_6	-0.3	-1.0	-0.7

Nomenclature

A	= total area, m^2
A_c	= cross section area of a single tube, m^2
a_B	= constant
$b, b_1, b_2, b_3,$	
b_4, b_G	= constants
c, C, C_3, C_4, C_c	= constants
d_h	= hydraulic diameter of compact heat exchanger, m
D	= tube hydraulic diameter diameter, m
f	= friction factor
G	= mass flux based on minimum flow area, $\text{kg}/\text{m}^2\text{s}$
H	= fin height, m
k_1, k_2, k_3, k_4, k_5	= constants
L	= channel length, m
m	= exponent in Blausius type friction factor
M	= number of data points
MAE	= mean absolute error
N	= number of fins per column
n	= constant
N_{row}	= number of tubes per row
N_t	= number of total tubes
Δp	= pressure drop, kPa
p_{exit}	= exit pressure, kPa
p_{in}	= inlet pressure, kPa
S_d	= diagonal pitch, m
S_L	= longitudinal pitch, m
S_T	= transverse pitch, m
Q	= volumetric flowrate, m^3/s
Re	= Reynolds number based on the pin fin hydraulic diameter, GD/μ
Re_d	= Reynolds number based on the hydraulic diameter of the channel, Gd_h/μ
w	= channel thickness, m

Greek

$\alpha_0, \alpha_1, \alpha_2, \alpha_3$	= constants
μ	= viscosity, kg/ms
ρ	= density, m^3/s
π_1	= first term of the right hand side in Eq. (13)

Table 9 MAE's of the new correlation for each device

Device	MAE (%)
1SDS	7.2
2SCL	11.5
3SCS	3.5
4ICL	2.7

π_2 = second term of the right hand side in Eq. (13)

Subscripts

- av = average
- exp = experimental
- f = frictional
- F = fluid
- min = minimum
- pred = predicted

References

- [1] Lossey M. W., Jackman J., Firebaugh S. L., and Schmidt M. A., Jensen K., 2002, "Design and fabrication of microfluidic devices for multiphase mixing and reaction," *J. Microelectromech. Syst.*, **11**(6), pp. 709–717.
- [2] Hitt, D. L., Zakrzewski, C. M., and Thomas, M. A., 2001, "MEMS-based Satellite Micropulsion via Catalyzed Hydrogen Peroxide Decomposition," *Smart Mater. Struct.*, **10**, pp. 1163–1175.
- [3] London, A., Development and Testing of a Microfabricated Bipropellant Rocket Engine, 2000, Ph.D. thesis, Massachusetts Institute of Technology, Boston, MA.
- [4] Christel, L. A., Petersen K., McMillan W., and Northrup M. A., 1999, "Rapid, Automated Nucleic Acid Probe Assays using Silicon Microstructures for Nucleic Acid Concentration," *J. Biomech. Eng.*, **121**, pp. 22–27.
- [5] Short, Jr., B. E., Raad P. E., and Price D. C., 2002, "Performance of Pin Fin Cast Aluminum Coldwalls, Part 1: Friction Factor Correlations," *J. Thermophys. Heat Transfer*, **16**(3), pp. 389–396.
- [6] Gaddis, E. S. and Gnielski, V., 1985, "Pressure Drop in Horizontal Cross Flow across Tube Bundles," *Int. Chem. Eng.*, **25**(1), pp. 1–15.
- [7] Sparrow, E. M. and Grannis, V. B., 1991, "Pressure Drop Characteristics of Heat Exchangers Consisting of Arrays of Diamond- Shaped Pin Fins," *Int. J. Heat Mass Transfer*, **34**(3), pp. 589–600.
- [8] Chyu, M. K., Hsing, Y. C., and Natarajan, V., 1998, "Convective Heat Transfer of Cubic Fin Arrays in a Narrow Channel," *J. Heat Transfer*, **120**, pp. 362–367.
- [9] Ruth, E. K., 1983, "Experiments on a Cross Flow Heat Exchanger With Tubes of Lenticular Shape," *J. Heat Transfer*, **105**, pp. 571–575.
- [10] Sara, O. N., 2003, "Performance Analysis of Rectangular Ducts With Staggered Square Pin Fins," *Energy Convers. Manage.*, **44**, pp. 1787–1803.
- [11] Lau, S. C., Kim, Y. S., and Han, J. C., 1985, "Effects of Fin Configuration and Entrance Length on Local Endwall Heat/Mass Transfer in a Pin Fin Channel," ASME Paper No.81-WA-HT-6.
- [12] Damerow, W. P., Murtaugh, J. C., and Burgraf, F., 1972, "Experimental and Analytical Investigation of the Coolant Flow Characteristics in Cooled Turbine Airfoils," NASA, CR-120883.
- [13] Metzger, D. E., Fan, Z. N., and Shepard, W. B., 1982b, "Pressure Loss and Heat Transfer Through Multiple Rows of Short Pin Fins," *Journal of Heat Transfer*, Vol. 3, edited by U. Grigull et al., Hemisphere, Washington, pp. 137–142.
- [14] Jacob, M., 1938, "Discussion-Heat Transfer and Flow Resistance in Cross Flow of Gases Over Tube Banks," *Mech. Eng. (Am. Soc. Mech. Eng.)*, **60**, pp. 381–392.
- [15] Armstrong, J. and Winstanley, D., 1988, "A Review of Staggered Array Pin Fin Heat Transfer for Turbine Cooling Applications," *ASME J. Turbomach.*, **110**, pp. 94–103.
- [16] Peng, Y., 1984, "Heat Transfer and Friction Loss Characteristics of Pin Fin Cooling Configurations," *ASME J. Eng. Gas Turbines Power*, **106**, pp. 246–251.
- [17] Sparrow, E. M. and Kang, S. S., 1985, "Longitudinally-finned Cross Flow Tube Banks and their Heat Transfer and Pressure Drop Characteristics," *Int. J. Heat Mass Transfer*, **28**(2), pp. 339–350.
- [18] Short, Jr., B. E., Price D. C., and Raad P. E., 2004, "Design of Cast Pin Fin Coldwalls for Air-Cooled Electronic Systems," *J. Electron. Packag.*, **126**, pp. 67–73.
- [19] Zukauskas, A. A., 1972, "Heat Transfer From Tubes in Cross Flow," *Advances in Heat Transfer*, Vol. 8, Academic, New York, pp. 93–160.
- [20] Kline, S. and McClintock, F. A., 1953, "Describing Uncertainties in Single-Sample Experiments," *Mech. Eng. (Am. Soc. Mech. Eng.)*, **75**(1), pp. 3–8.
- [21] Gunter, A. Y. and Shaw, W. A., 1945, "A General Correlation of Friction Factors for Various Types of Surfaces in Cross Flow," *Mech. Eng. (Am. Soc. Mech. Eng.)*, **67**, pp. 643–660.
- [22] Taborak, J., 1983, "Shell-and-Tube Heat Exchangers: Single phase Flow," *Handbook of Heat Exchanger Design*, Hemisphere, New York, Chap. 3.3.
- [23] Moores, K. A. and Joshi, Y. K., 2003, "Effect of Tip Clearance on the Thermal and Hydrodynamic Performance of a Shrouded Pin Fin Array," *J. Heat Transfer*, **125**, pp. 999–1006.
- [24] Chilton, T. H. and Generaux, R. P., 1933, "Pressure Drop Across Tube Banks," *Trans. Am. Inst. Chem. Eng.*, **29**, pp. 161–173.
- [25] Bergelin, O. P., Colburn, A. P., and Hull, H. L., 1950, "Heat Transfer and Pressure Drop during Viscous Flow across Unbaffled Tube Banks," *Engineering Experimental Station, Bulletin No.2*, University of Delaware, Newark, DE.
- [26] Kast, W., 1974, *Druckverlust bei der Strömung quer zu Rohrbündeln (Pressure Drop in Cross Flow across Tube Bundles)*, VDI-Wärmeatlas, Section Ld, 2nd ed.
- [27] Mathews, J. H., 1992, *Numerical Methods for Mathematics, Science, and Engineering*, Prentice Hall, New Jersey, pp. 258–280.